# Defects in Irradiated Silicon. I. Electron Spin Resonance of the Si-$A$ Center

G. D. WATKINS AND J. W. CORBETT
*General Electric Research Laboratory, Schenectady, New York*
(Received October 7, 1960)

The Si—$A$ center is a major, radiation-damage defect produced in "pulled" silicon by a room temperature irradiation. As a result of studies described in this paper (I), and the following one (II), it is concluded that this center is a lattice vacancy with an oxygen atom impurity bridging two of the four broken bonds associated with the vacancy. Spin resonance and electrical activity arise from an electron trapped in the other two bonds. In this paper (I), the spin resonance studies are described. A molecular orbital treatment of the trapped electron wave-function satisfactorily accounts for the observed $g$ tensor, as well as the hyperfine interaction observed with neighboring 4.7% abundant $Si^{29}$ nuclei. Study of the changes in the spectrum of a sample subjected to uniaxial stress are also described. Under stress, the amplitudes of the individual resonance components (which correspond to different orientations of the defect in the crystal) are observed to change. This results from (1) electronic redistribution of the trapped electrons among the defects, and (2) thermally activated reorientation of the defects themselves under the applied stress. These two effects are separated and a quantitative study of their magnitudes and signs, as well as their rates, is given. The results confirm many of the important microscopic features of the model.

## I. INTRODUCTION

CONSIDERABLE effort has gone into the study of radiation damage in the elemental semiconductors, germanium and silicon, over the past ten years.[1] Much has been learned about the changes in the physical properties of these materials as a result of irradiation, but rather little has emerged by way of understanding of the basic processes involved. In many cases it has been possible to identify specific electrical, optical, and mechanical property changes as arising from a specific defect that has been formed. However, in most cases, it has not been possible to identify the defect involved. The reason for this failure is that apparently the damage process is rather complex and it has not been possible so far to unravel this complexity with the macroscopic measurement techniques used in the past.

Recently, several workers[2–6] have reported electron spin resonance studies in irradiated silicon. A number of well-resolved spectra have been observed indicating that many of the defects produced in this material can be studied by this powerful microscopic technique. Already one surprise has emerged from these studies. That is the discovery[6] of the hitherto unsuspected role of impurities in room temperature irradiated silicon. These results indicated that the interstitials or vacancies (or both) are mobile below room temperature and that the defects remaining after a room temperature irradiation result from the trapping of these primary defects by impurity atoms. Most previous workers had assumed that the defects stable at room temperature were the primary ones, (i.e., interstitials, vacancies, close pairs).

In this paper, we will describe a detailed spin resonance study of one such defect stable at room temperature. This defect, the Si—$A$ center,[7] is a major defect produced by high-energy electron irradiation in pulled[8] silicon. It was first observed in spin resonance by Bemski, Feher, and Gere.[2] In a subsequent study,[6] we have demonstrated that it is also the same defect as one previously studied by Wertheim[9] and Hill[10] in electrical measurements (a net acceptor level at $E_c-0.17$ ev). In this study[6] we also discovered that oxygen (normally present in pulled silicon in a concentration of approximately $10^{18}$ cm$^{-3}$) is necessary for the formation of this defect. The role of oxygen has subsequently been confirmed by others in spin resonance[5] and in electrical measurements.[11]

As a result of the spin resonance studies outlined in this paper and the infrared studies described in the

[1] For a recent review of radiation effects in semiconductors, see J. Appl. Phys. **30**, 1117–1322 (1959), containing papers and discussions presented at the Conference on Radiation Effects in Semiconductors, Gatlinburg, Tennessee, May, 1959.
[2] G. Bemski, G. Feher, and E. Gere, Bull. Am. Phys. Soc. **3**, 135 (1958).
[3] G. D. Watkins, J. W. Corbett, and R. M. Walker, Bull. Am. Phys. Soc. **4**, 159 (1959).
[4] E. Schulz-DuBois, M. Nisenoff, H. Y. Fan, and K. Lark-Horovitz, Phys. Rev. **98**, 1561(A) (1955); M. Nisenoff and H. Y. Fan, Bull. Am. Phys. Soc. **4**, 159 (1959).
[5] G. Bemski, J. Appl. Phys. **30**, 1195 (1959).
[6] G. D. Watkins, J. W. Corbett, and R. M. Walker, J. Appl. Phys. **30**, 1198 (1959).
[7] We feel the question of nomenclature deserves a few remarks. It is clear experimentally that there are many distinct spin resonance spectra (we have already found approximately 20) which can be observed in irradiated silicon and presumably correspond to many different defect centers. (Some may be different charge states of the same defect.) Ideally each spectrum should be labeled in a manner descriptive of its microscopic constitution but this knowledge does not come until after protracted study of the spectrum and its correlative data, and even then with varying degrees of certainty. We had consequently taken to labeling the centers alphabetically, whence the $A$, $E$, etc., centers in footnote 6. This system runs into trouble very quickly when it encounters already existing terminology (e.g., the $F$, $H$, $M$, etc., centers occur in the alkali halides). For this reason, and since we hope other systems—Ge, InSb, etc.—will be as fruitful as Si, we suggest for general usage the designation of Si—$A$, Si—$E$, etc., for the centers we have previously labeled the $A$, $E$, etc. centers. In the remainder of the paper, however, we will retain the simpler label, $A$ center, since it is clear this paper refers only to silicon.
[8] Silicon grown by pulling a single crystal from the melt. The melt is contained in a quartz crucible.
[9] G. K. Wertheim, Phys. Rev. **105**, 1730 (1957); **110**, 1272 (1958).
[10] D. E. Hill, Phys. Rev. **114**, 1414 (1959).
[11] G. K. Wertheim and D. N. E. Buchanan, J. Appl. Phys. **30**, 1232 (1959); E. Sonder and L. C. Templeton, Bull. Am. Phys. Soc. **5**, 196 (1960).

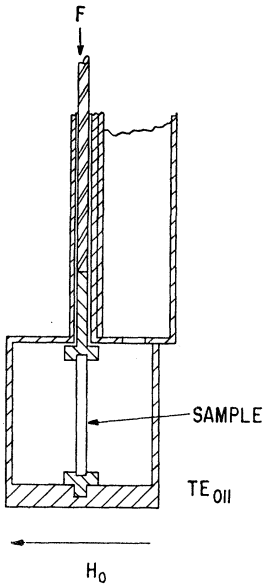


FIG. 1. Method of applying uniaxial stress to the sample. The sample is held between two Teflon cups in the center of the cylindrical microwave cavity. A simple lever with weights outside the cryostat supplies the force to a stainless steel rod which transmits the force to the Teflon cups.

following paper,[12] we are able to conclude that the $A$ center is a single oxygen atom in a lattice vacancy. It is, therefore, presumably formed when a mobile vacancy is trapped by an interstitial oxygen atom.[13] In this first paper the evidence which is based upon spin resonance studies will be presented. From the analysis of the spin resonance spectrum, it is possible to propose a detailed model for the defect. In addition, experiments will be described in which uniaxial stress is applied to the sample. The changes in the spin resonance spectrum accompanying the stress are interpreted to confirm several important features of the model.

It is not possible to detect the presence of the oxygen atom directly in the spin resonance. Its presence is only inferred. However, in the following paper,[12] an infrared absorption band at 12 $\mu$ is identified as arising from the vibration of this oxygen atom. In this second paper, a detailed comparison of the infrared and spin resonance studies proves the presence of the oxygen atom and also confirms the detailed model as to how the oxygen is incorporated into the defect.

## II. EXPERIMENTAL PROCEDURE

The silicon samples studied were $n$ type (phosphorus $\sim 10^{15}-10^{16}/\text{cm}^3$). They were grown in an argon atmosphere and were rotated while pulling from the melt, the melt being contained in a quartz crucible.[14] The samples were 0.095 in. thick and were irradiated equally on both sides at room temperature by 1.5 Mev electrons from a resonance transformer accelerator. The current was adjusted to 2.5 $\mu$a/cm$^2$, the maximum temperature rise in the sample being about 25°C.

Spin resonance was studied using a balanced bolometer spectrometer[15] at 20 kMc. Magnetic field modulation and lock-in detection at 94 cps were employed. The measurements were made in dispersion. At 20°K rapid passage effects[16,17] gave absorptionlike spectra. The studies at higher temperatures gave derivative of dispersion curves.

Uniaxial stress was supplied to the sample as shown in Fig. 1. The sample was placed between two Teflon cups (which become quite hard at low temperatures). A simple lever with weights outside the cryostat supplied the force to a stainless steel rod which entered the cryostat through an "O" ring and transmitted the force to the Teflon cups.

Studies vs temperature were made below 77°K by first cooling to 20°K, expelling the liquid $H_2$ coolant, and observing as the cavity plus cryostat warmed up to the 77°K of the cryostat heat shield. For temperatures above 77°K, a heater connected to the waveguide approximately 6 in. above the cavity was used. Temperature was monitored by a copper-constantan thermocouple on the cavity.

## III. GENERAL RESULTS AND DISCUSSIONS

### A. Experimental Results

#### 1. *Summary of Previous Work*

Previous studies[6] have shown the following:

1. The $A$ center is an electron trap ($0.17\pm0.01$) ev below the conduction band (see Fig. 2). It is, therefore, the same "net-acceptor" defect found to be the dominant defect produced in nondegenerate $n$-type pulled silicon by Wertheim[9] and Hill[10] in electrical measurements. Spin resonance is observed only for defects that have trapped an electron. The experiment is therefore done in $n$-type silicon, the purpose of the donor (phosphorus in Fig. 2) being to supply electrons to the deeper lying $A$ center.

2. The $A$ center is not a primary defect (i.e., interstitial, vacancy, close pair, etc.) as was demonstrated by the fact that no $A$ centers are observed after a 20°K irradiation. They do appear upon subsequent annealing.[18]

[12] J. W. Corbett, G. D. Watkins, R. M. Chrenko, and R. S. McDonald, Phys. Rev. **121**, 1015 (1961).

[13] This model was suggested by the authors as part of the oral presentation in footnote 3. It has also been suggested by Bemski.[5]

[14] These samples were kindly supplied by Dr. R. O. Carlson.

[15] See, for instance, G. Feher, Bell System Tech. J. **36**, 449 (1957).

[16] A. M. Portis, Phys. Rev. **100**, 1219 (1955); Technical Note No. 1, Sarah Mellon Scaife Radiation Laboratory, University of Pittsburgh, Nov. 15, 1955 (unpublished).

[17] G. Feher, Phys. Rev. **114**, 1219 (1959).

[18] An interesting feature is that the number of centers formed after a low temperature irradiation and anneal to room temperature is only a few percent of what is formed in an equivalent room temperature irradiation. This effect has also been observed by Wertheim[9,19] and Hill[10] in silicon, and by Brown and Augustyniak[20] in germanium, using electrical measurements as their monitor. Bemski[5] has also observed lower $A$ center production in spin resonance after a 90°K irradiation and anneal. The reason for this effect is not understood at present, although one explanation has been suggested.[19]

[19] G. K. Wertheim, Phys. Rev. **115**, 568 (1959).

[20] W. L. Brown and W. M. Augustyniak, J. Appl. Phys. **30**, 1300 (1959).

3. Hyperfine interaction with 4.7% abundant $Si^{29}$ has shown that the trapped electron is highly localized on two silicon atoms. The triangular symmetry of the center as deduced from the $g$ tensor and the anisotropy of the $Si^{29}$ hf interactions is shown in Fig. 3.

4. Oxygen, normally present in a concentration of approximately $10^{18}/cm^3$ in pulled silicon,[21] appears necessary for the formation of the $A$ center. In vacuum floating zone silicon,[22] which may contain a factor of $\geqslant 100$ less oxygen,[21] the production rate of the $A$ center is observed to be very low.[23]

### 2. *Role of Oxygen*

Since there may be differences between pulled and vacuum floating zone crystals other than oxygen content (dislocation content, for instance), it was desirable to demonstrate the role of oxygen in another way. This was done as follows: Two crystals were cut from the same boule of a pulled $n$-type crystal. One was heat treated at 1000°C for 100 hr, to reduce the concentration of oxygen in solid solution by precipitation.[24,25] The intensity of the 9-$\mu$ absorption band associated with oxygen in solution indicated that it had been reduced by a factor of 7.5. The $A$ center production rate in this sample was measured and was found to be a factor of 2.5 below the untreated sample. The fact that the $A$ center production rate can be altered in a way that can be correlated with the dissolved oxygen gives additional support as to the role of oxygen.[26]

### 3. *Spin Resonance Spectrum*

The spectrum can be described by the spin Hamiltonian

$$\mathcal{H}=\beta\mathbf{H}\cdot\mathbf{g}\cdot\mathbf{S}+\sum_j \mathbf{I}_j\cdot\mathbf{A}_j\cdot\mathbf{S}, \qquad (1)$$

with $S=\frac{1}{2}$. The first term is the interaction of the spin with the external magnetic field, and the values of the $g$ tensor along the principal axes (see Fig. 3) are measured to be

$$g_1=2.0093\pm0.0003,$$
$$g_2=2.0025\pm0.0003,$$
$$g_3=2.0031\pm0.0003.$$

The second term in Eq. (1) describes the magnetic interaction of the spin with nearby $Si^{29}$ nuclei (4.7% abundant, $I=\frac{1}{2}$). $\mathbf{A}_j$ is the corresponding hyperfine tensor for the $j$th lattice site.

In addition to the large $Si^{29}$ hyperfine interaction at two atom sites mentioned previously, interaction at four other nonequivalent sets of atom sites are resolved[27] and the results are summarized in Table I. These sites are labeled $A$ through $E$ in order of decreasing interaction and the corresponding multiplets in the spectrum are indicated in Fig. 4. The number of equivalent atom sites in each set is estimated by the relative intensity of each satellite.

For each site the hyperfine interaction is found to be axially symmetric and therefore described by the magnitude of $\mathbf{A}$ parallel ($A_{\parallel}$) and perpendicular ($A_{\perp}$) to its axis. Each set of equivalent sites may be further divided in two in that half of the sites have their axis closely along the $[1\bar{1}1]$ axis, the other half along the $[11\bar{1}]$ for the center depicted in Fig. 3.

Careful analysis of the hyperfine interaction at the $A$ sites reveals that the hyperfine axes are $\epsilon=0.8\mp0.2°$ away from the $[1\bar{1}1]$ and $[11\bar{1}]$ axes as shown in Fig. 3. They are still in the (011) plane but rotated toward the [100] direction such as to make the angle between the two hyperfine axes slightly less than the tetrahedral angle. The accuracy of measurement for the other sets of sites was not sufficient to detect any departure from the indicated axes.

A search for the hyperfine structure associated with

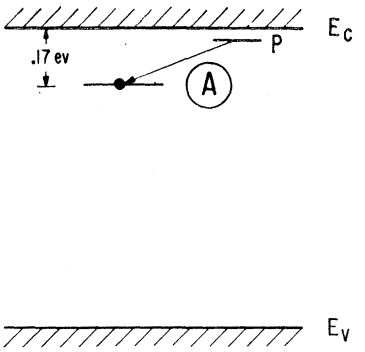


FIG. 2. The $A$ center is an electron trap ("net-acceptor") at ($E_c-0.17$ ev). The experiment is performed in phosphorus-doped silicon, the purpose of the donor being to supply electrons to the $A$ center. Spin resonance is observed only for those defects which have trapped an electron.

[21] W. Kaiser, P. H. Keck, and C. F. Lange, Phys. Rev. **101**, 1264 (1956).

[22] Obtained from the Merck Chemical Company.

[23] In vacuum floating zone silicon, different spin resonance centers are observed. The dominant center, designated the $E$ center, we identify as a vacancy trapped next to a substitutional phosphorus; it will be treated in detail in a subsequent paper. In light of the identification we will make in the present paper of the $A$ center as a vacancy trapped by an interstitial oxygen, the $E$ center completes the picture as to where the vacancy goes when there is no oxygen to trap it.

[24] W. Kaiser, Phys. Rev. **105**, 1751 (1957).

[25] H. J. Hrostowski and R. H. Kaiser, J. Phys. Chem. Solids **9**, 214 (1959).

[26] One does not expect an exact one-to-one correspondence between the dissolved oxygen content and the $A$ center production rate. In fact, for us to get a change at all in the production rate, some other defects must be present to compete for the trapping of the mobile primary defects (vacancies). Oxygen is also present in precipitated form in these crystals, suggesting that these precipitates are the competing traps.

[27] Previous studies at 20°K[6] and at lower temperatures[5] did not resolve these additional hyperfine interactions. At these low temperatures, rapid passage effects[16,17] give a recorded absorptionlike spectrum. The derivative of dispersion shown in Fig. 4 at approximately 40°K is similar to a second derivative of the absorption curve and, as a result, gives much higher resolution.

TABLE I. Observed $Si^{29}$ hyperfine interaction constants for the nonequivalent atom sites in the vicinity of an $A$ center. The interactions are axially symmetric and half of the axes for each set are closely along the $[1\bar{1}1]$ axis, the other half along the $[11\bar{1}]$ axis for the center depicted in Fig. 3. The accuracy in the $A$ is $\mp 0.5(10^{-4})$ $cm^{-1}$.

| Atom site | No. of equivalent sites | $\lvert A_{\parallel}\rvert$ ($10^{-4}$ $cm^{-1}$) | $\lvert A_{\perp}\rvert$ ($10^{-4}$ $cm^{-1}$) |
|---|---|---|---|
| $A$ | 2 | 153.0 | 128.8 |
| $B$ | 2 | 16.0 | 12.0 |
| $C$ | 2 | 10.6 | 7.9 |
| $D$ | 4–6 | 7.0 | 5.2 |
| $E$ | 4–6 | 2.5 | 2.5 |

$O^{17}$ ($I=\frac{5}{2}$) was made in a sample in which the dissolved oxygen had been enriched[28] to approximately 1.5% $O^{17}$. Originally $p$ type, the material was converted to $n$ type by diffusing lithium into it[28] and it was subsequently irradiated. The resulting $A$ center resonance was of sufficient intensity to observe the $O^{17}$ hfs if it were large enough to emerge from the $Si^{29}$ hfs ($B$ through $E$ sites) in close to the lines. No hfs was observed, indicating that if an oxygen atom is involved in the $A$ center, $\lvert A(O^{17})\rvert \lesssim 5\times 10^{-4}$ $cm^{-1}$.[29]

## B. Discussion

### 1. *Model*

In order to interpret the experimental results it will simplify matters to present an approximate description of the model of the defect at the outset. This is shown in Fig. 5. It is comprised of a single oxygen atom in a lattice vacancy. We can visualize the construction of this defect as follows: Initially there are four broken bonds around a vacancy, one for each of the four silicon atoms surrounding it. The role of the oxygen is to bridge two of these broken bonds, forming an Si—O—Si "molecule." The remaining two silicon atoms pull together to form a Si—Si molecular bond. In the neutral state this defect is not paramagnetic, all electrons being paired off. Paramagnetism and spin resonance arise from an additional electron which is trapped in the Si—Si molecular bond as shown.

A more detailed consideration of the Si—Si bond is shown in Fig. 6. The defect is viewed from a different aspect than in Figs. 3 and 5, in order to show the Si—Si bond in the plane of the paper. Consider the construction of this bond as follows: In the absence of overlap, the broken bond orbitals on $Si_A$ and $Si_{A'}$ are given by $\psi_A$ and $\psi_{A'}$, and their energy levels, let us assume, lie near the middle of the forbidden gap. In the presence of overlap, the molecular orbitals are split into a bonding and an antibonding orbital as shown, the splitting being proportional to the overlap integral or bond energy. For not too strong an overlap, the linear combination of atomic orbitals (LCAO) shown in Fig. 6 should represent a good approximation. In the neutral state, the two electrons (one contributed by each atom) are paired off in the bonding orbital. The additional trapped electron goes into the antibonding orbital shown in the figure to be the level at ($E_c-0.17$ ev). The position of $E_v$ with respect to the other orbitals is not known and is therefore shown dashed. The bonding orbital may well be below $E_v$.

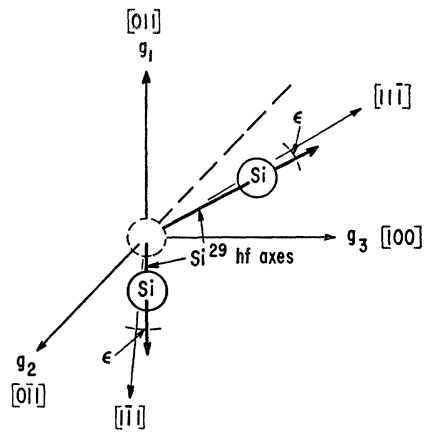


FIG. 3. The $g$-tensor and hyperfine axes of the $A$ center.

One might ask why a negative antibonding charge state is stable. To answer this, one must keep in mind the fact that an electron in the conduction band is also in a negative antibonding state, and stability really means only that the negative antibonding state on the $A$ center is lower in energy. With this in mind, there are several possible reasons which may contribute to this stability: (1) The $AA'$ orbital is less antibonding than those of the conduction band because it is associated with a weaker bond. (The conduction band arises from the strong normal Si—Si bond of the lattice.) (2) In forming the $AA'$ bond there is considerable strain in the surrounding lattice resulting from the pulling of the two Si atoms together. When an antibonding electron is added, the atoms relax back toward their normal lattice positions, lowering this strain energy. (3) As has been considered by James and Lark-Horovitz,[30] in order to minimize the disturbance to the valence band wave functions, there is a tendency to extend the crystal wave functions through a defect. Since the $A$ center core is electron deficient, this also represents a driving force toward the capture of an extra electron. It would be difficult to assess the relative importance of these effects (which are not entirely separable) but we suggest that their combined effect is to make the additional antibonding electron at the $A$ center stable at ($E_c-0.17$ ev).

[28] This sample, kindly supplied by Dr. H. J. Hrostowski, is the same sample studied in the following paper where the accompanying $O^{18}$ isotope is studied. The lithium doping was kindly performed by Dr. E. M. Pell.

[29] G. Bemski (unpublished) had previously attempted to observe the $O^{17}$ hfs in a sample from the same boule, also with a negative result.

[30] H. M. James and K. Lark-Horovitz, Z. physik. Chemie **198**, 107 (1951).

Spin resonance thus arises from the electron in this antibonding orbital. Comparison of Figs. 3 and 5 shows that this model satisfies many of the essential features deduced from the resonance: (1) The electron is primarily localized on two silicon atoms. (2) The hyperfine axes at the silicon sites point toward the center of the vacancy, reflecting the symmetry of the broken bond atomic orbitals which make up the molecular orbital. (3) The principal symmetry axes of this orbital agree with the principal axes of the $g$ tensor.

In the next two sections, the hyperfine interactions and the $g$ tensor will be considered quantitatively in terms of this model. Consideration of the additional hyperfine interactions, $B$ through $E$ (see Table I), will allow an extension of the model to include the electronic overlap with these more distant sites.

### 2. *Hyperfine Interactions*

The hyperfine interaction at a nuclear site arises from magnetic interaction between the nucleus and the surrounding electrons. This is given by[31]

$$\mathcal{H}=2\gamma\beta\beta_N\sum_k\left\{\frac{3(\mathbf{r}_k\cdot\mathbf{s}_k)(\mathbf{r}_k\cdot\mathbf{I})}{r_k^5}+\frac{(\mathbf{l}_k-\mathbf{s}_k)\cdot\mathbf{I}}{r_k^3}+\frac{8\pi}{3}\delta(\mathbf{r}_k)(\mathbf{s}_k\cdot\mathbf{I})\right\}, \quad (2)$$

where $\gamma$ is the nuclear $g$ value, $\beta$ the Bohr magneton, $\beta_N$ the nuclear magneton, $\mathbf{I}$ the nuclear spin, $\mathbf{s}_k$ the spin and $\mathbf{l}_k$ the orbital angular momentum of the $k$th electron, and $\mathbf{r}_k$ is the radius vector of this electron from the nucleus. Averaged over the many-electron wave function which describes the spin density of the paramagnetic center, the result can be expressed as

$$\mathcal{H}_{hf}=\mathbf{I}\cdot\mathbf{A}\cdot\mathbf{S}, \quad (3)$$

as in Eq. (1). For a wave function which is axially symmetric in the vicinity of the nucleus, the principal values of $\mathbf{A}$ are given by

$$A_{\parallel}=a+2b, \qquad A_{\perp}=a-b, \quad (4)$$

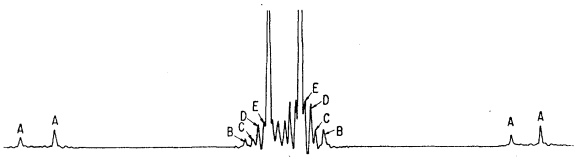


FIG. 4. $A$ center spectrum at approximately 40°K with the magnetic field $H\|\langle 100\rangle$. Resolved $Si^{29}$ hyperfine multiplets for five nonequivalent sets of atom sites in the vicinity of the center (labeled $A$ through $E$) are observed.

[31] A. Abragam and M. H. L. Pryce, Proc. Roy. Soc. (London) **A205**, 135 (1951).

where[32–34]

$$a=\frac{16\pi}{3S}\gamma\beta\beta_N\langle\textstyle\sum_k\delta(\mathbf{r}_k)s_{kz}\rangle_{S_z=S},$$
$$b=\frac{\gamma\beta\beta_N}{S}\left\langle\sum_k\left(\frac{3\cos^2\theta_k-1}{r_k^3}\right)s_{kz}\right\rangle_{S_z=S}. \quad (5)$$

Here $\theta_k$ is the angle between $\mathbf{r}_k$ and the axis of symmetry ($z$ axis).

Equation (5), in summing over all electrons, expresses the fact that in addition to the direct interaction between the nucleus and an unpaired electron, there is an indirect interaction via the other electrons in the solid, (i.e., the magnetic field seen by the nucleus arises both directly from the spin of the unpaired electron and from the magnetization it induces in the closed shell bonding and ion core electrons[35]). The indirect interaction is expected to be small with respect to the direct interaction. However, in special cases where the direct interaction is small but the unpaired electron wave function has a sizeable magnitude in the immediate vicinity (such as at a node in the wave function), the indirect interactions may be important.[36] As a result, in the development to follow, we will consider only the direct interactions. We will keep in mind, however, the possibility that when the observed interactions are small, they may be indirect in origin.

Let us now consider the wave function for the unpaired electron. We assume it can be constructed as a linear combination of atomic orbitals (LCAO) centered on silicon sites in the vicinity of the vacancy,

$$\Psi=\textstyle\sum_j\eta_j\psi_j. \quad (6)$$

Here $\psi_j$ is an atomic orbital at the $j$th site and we construct it as a hybrid $3s3p$ orbital given by

$$\psi_j=\alpha_j(\psi_{3s})_j+\beta_j(\psi_{3p})_j, \quad (7)$$

[32] The contribution of $\mathbf{l}_k$ in Eq. (2) has not been included. The small observed $g$ shifts from the free electron value assure that this contribution is negligible.

[33] A. Abragam, J. Horowitz, and M. H. L. Pryce, Proc. Roy. Soc. (London) **A230**, 169 (1955).

[34] H. M. McConnell and D. B. Chesnut, J. Chem. Phys. **28**, 107 (1958).

[35] What we call the wave function of the unpaired electron is, of course, somewhat arbitrary. One could construct a one-electron wave function which completely describes all of the spin density. We would then have only a "direct" interaction. However, for this wave function, the spin and position dependent parts would not be separable. That is, the spin function would be position dependent. For this reason, it is more convenient to consider one-electron wave functions for which the spin functions are position independent. We consider an unpaired electron as localized in one such wave function; the role of the other $k$ electrons in the interaction is therefore "indirect."

[36] Examples of this are the origins of the isotropic interaction [the $a$ in Eq. (5)] for the transition elements[33,37,38] and for the in-plane hydrogen atoms in aromatic organic radicals.[34] In both cases the "direct" interaction is zero.

[37] J. H. Wood and G. W. Pratt, Jr., Phys. Rev. **107**, 995 (1957).

[38] V. Heine, Phys. Rev. **107**, 1002 (1957).

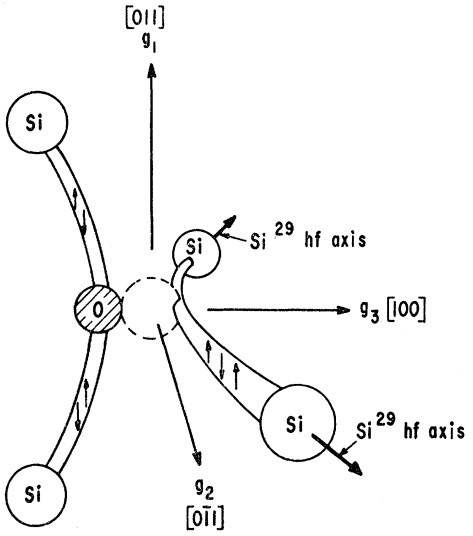


FIG. 5. Model of the $A$ center as a substitutional oxygen atom. The oxygen atom bonds between two of the four neighboring silicon atoms, and the remaining two silicon atoms pull together to form a covalent bond. Spin resonance arises from an additional electron which is trapped in the Si—Si molecular bond as shown. The $g$ tensor and hyperfine axes are indicated.

where, in each case, the $p$ orbital is directed along the hyperfine symmetry axis for the $j$th site.[39] Ignoring overlap, normalization requires

$$\alpha_j^2+\beta_j^2=1, \tag{8a}$$

$$\sum \eta_j^2=1. \tag{8b}$$

For such a molecular orbital, the hyperfine interaction at the $j$th site will be determined primarily by the atomic orbital $\psi_j$ at that site. With Eq. (5), this gives

$$\begin{aligned} a_j &\cong (16\pi/3)\gamma\beta\beta_N\alpha_j^2\eta_j^2|\psi_{3s}(0)|^2, \\ b_j &\cong \tfrac{4}{5}\gamma\beta\beta_N\beta_j^2\eta_j^2\langle r^{-3}\rangle_{3p}. \end{aligned} \tag{9}$$

Therefore, we are led to conclude that since $\gamma$ for $Si^{29}$ is negative, both $a_j$ and $b_j$ are negative. As a result, even though only $|A_{\parallel}|_j$ and $|A_{\perp}|_j$ are determined experimentally, knowing the signs of $a_j$ and $b_j$, we can determine $a_j$ and $b_j$ from Eq. (4) unambiguously. Assuming negative signs for all sites, the results are given in Table II. [Indirect interactions which are not included in Eq. (9) can give contributions of opposite sign to $a_j$ and $b_j$. As a result, the assumption of negative signs for the more distant $B$ through $E$ sites may be in error. The consequences of this will be discussed at the end of this section.]

We can make an estimate of $|\psi_{3s}(0)|^2$ and $\langle r^{-3}\rangle_{3p}$ from Hartree functions. Table III gives a summary of the results calculated from available published tabulations. (The estimate for $Si^0$ was obtained from experimental fine structure constants.) We are dealing with an extra electron on a neutral bonded Si atom and we might expect the values for $Si^-$ to apply to our case. However, molecular binding tends to pull the electron density of the valence electrons away from the core and may reduce their shielding effect somewhat. The correct values may be closer to those for the free $Si^0$ atom. In Table III the shielding effect of these valence electrons is apparent. Unfortunately, the calculations by the different workers were done with somewhat differing methods and only the trend is probably meaningful. Hartree, Hartree, and Manning[40] tabulated both the $3s$ and $3p$ functions for $Si^{3+}$ and the ratio of $|\psi_{3s}(0)|^2$ to $\langle r^{-3}\rangle_{3p}=1.4$ probably is meaningful. Since both $|\psi_{3s}(0)|^2$ and $\langle r^{-3}\rangle_{3p}$ are expected to vary with charge state in somewhat the same fashion, we make the assumption that this ratio also applies for the orbitals on the bonded silicon atoms with which we deal. If we use this, with the normalization requirement of Eq. (8a), the values $\alpha_j^2$ and $\beta_j^2$ can be determined for each site, and are as given in Table II. With the normalization requirement of Eq. (8b), the values of $\eta_A^2$, $\eta_B^2$, etc. can be determined and are also included.[41] (An average value of 5 was taken for the number of equivalent $D$ and $E$ sites in this calculation. The symmetry of the defect suggests that each must be an even number, either 4 or 6, but the final values of $\eta^2$ are rather insensitive to the choice.)

We have thus determined $\alpha_j^2$, $\beta_j^2$, and $\eta_j^2$ for each site assuming only: (1) the LCAO wave function of Eqs. (6) and (7) for the electron, (2) the ratio of $|\psi_{3s}(0)|^2$ to $\langle r^{-3}\rangle_{3p}=1.4$, and (3) direct hyperfine interactions only. We may now determine $|\psi_{3s}(0)|^2$ using Eq. (9); this result, along with the corresponding value for $\langle r^{-3}\rangle_{3p}$, is

TABLE II. Hyperfine parameters ($a_j$ and $b_j$) and the corresponding molecular wave-function coefficients ($\alpha_j^2$, $\beta_j^2$, and $\eta_j^2$) calculated from the observed hyperfine interaction constants for the nonequivalent atom sites in the vicinity of the $A$ center. It has been assumed that the hyperfine interactions are direct in origin, giving negative signs for $a_j$ and $b_j$.

| Atom site | $a_j$ ($10^{-4}$ cm$^{-1}$) | $b_j$ ($10^{-4}$ cm$^{-1}$) | $\alpha_j^2$ | $\beta_j^2$ | $\eta_j^2$ |
|---|---|---|---|---|---|
| $A$ | −136.8 | −8.1 | 0.37 | 0.63 | 0.355 |
| $B$ | (−)13.3 | (−)1.3 | 0.26 | 0.74 | 0.049 |
| $C$ | (−)8.8 | (−)0.9 | 0.25 | 0.75 | 0.034 |
| $D$ | (−)5.8 | (−)0.6 | 0.25 | 0.75 | 0.022 |
| $E$ | (−)2.5 | ∼0 | ∼1 | ∼0 | 0.002 |

[39] That is, $m_l=0$ along the axis of symmetry. Such a form is predicted by the model of Figs. 5 and 6 for the $A$ sites, where the orbital involved is a broken tetrahedral bonding orbital. For the more distant sites, this form is also reasonable in that one can consider these orbitals as arising as a result of admixture of conduction and valence band wave functions into the localized Si—Si molecular orbital. The conduction and valence bands are also made up primarily of $3s$ and $3p$ functions.

[40] W. Hartree, D. R. Hartree, and M. F. Manning, Phys. Rev. **60**, 857 (1941).

[41] We here neglect as small the fraction of the wave function which is spread out over still more distant sites for which the hyperfine structure is not resolved. If the wave function were spread over a large number of such sites, a significant fraction of the wave function could be involved and still not contribute much to the residual width of the line. However, we do not anticipate this since the defect is charged negatively and there is no Coulomb attractive center.

TABLE III. Available theoretical and experimental estimates of $|\psi_{3s}(0)|^2$ and $\langle r^{-3}\rangle_{3p}$ for different charge states of silicon compared with the values determined from the $A$ center analysis. The indicated values were determined from (H) tabulated Hartree functions, (HF) tabulated Hartree-Fock functions, (FS) experimental fine structure constants, and (A) $A$ center analysis.

| Charge state | $\lvert\psi_{3s}(0)\rvert^2$ ($10^{24}$ cm$^{-3}$) | $\langle r^{-3}\rangle_{3p}$ ($10^{24}$ cm$^{-3}$) |
|---|---|---|
| $Si^{3+}$ | 38.5(HF),[a] 42.9(H)[b] | 27.6(HF)[a] |
| $Si^{2+}$ | 36.4(H)[b] | ··· |
| $Si^{+}$ | ··· | 23(HF)[c] |
| $Si^{0}$ | ··· | 15.7(FS)[d] |
| bonded $Si^{-}$ | 24(A) | 17(A) |

[a] W. Hartree, D. R. Hartree, and M. F. Manning, Phys. Rev. **60**, 857 (1941).
[b] H. L. Donley, Phys. Rev. **50**, 1012 (1936).
[c] L. Biermann and K. Lübeck, Z. Astrophys. **25**, 325 (1948).
[d] R. G. Barnes and W. V. Smith, Phys. Rev. **93**, 95 (1954).

given in Table III. The values are in satisfactory agreement with what one would estimate for neutral silicon.

It is interesting to note that for the $B$, $C$, and $D$ sites, $\alpha^2=\frac{1}{4}$, $\beta^2=\frac{3}{4}$, which gives the tetrahedral $sp^3$ orbitals of Pauling.[42] This physically plausible result serves to confirm the choice of the relative signs of $a_j$ and $b_j$. (If opposite signs were chosen, $\alpha^2\sim0.01$, $\beta^2\sim0.99$.) We therefore conclude that the magnitudes and relative signs (equal) of $a_j$ and $b_j$ are correct. We have no check on the signs of these constants; the negative values, predicted by the direct interaction, are therefore bracketed in Table II. The calculated $\eta_j^2$ value for any site has meaning only if the direct interaction is dominant. If one of these sites were at a node in the wave function, the values of $a_j$ and $b_j$ could be positive and the corresponding value of $\eta_j^2$ incorrect. However, since only a small percentage of the wave function is involved, this would not alter the other values of $\eta_j^2$ significantly.

The orbitals on the $A$ sites have somewhat larger $s$ character, being closer to an $sp^2$ orbital.[42] This is consistent with the distorted position of this silicon atom as can be seen as follows: Increased $s$ character in this orbital means reduced $s$ character in the orbitals which bond the $A$ silicon to its three neighbors. Reducing their $s$ character can easily be shown to cause these three directed orbitals to close slightly, the angles between them decreasing from the original tetrahedral angles. This is consistent with the required bond directions from the distorted silicon site, it being pulled away from its three neighbors toward the vacancy by the $Si_A-Si_{A'}$ molecular bond.

The failure to observe hyperfine interaction with $O^{17}$ can be explained as follows: The electronic wave function is an antibonding orbital and antisymmetric about the plane midway between the $A$ and $A'$ sites. The oxygen atom, in this plane, is therefore at a node in the wave function and only a small interaction would be expected.

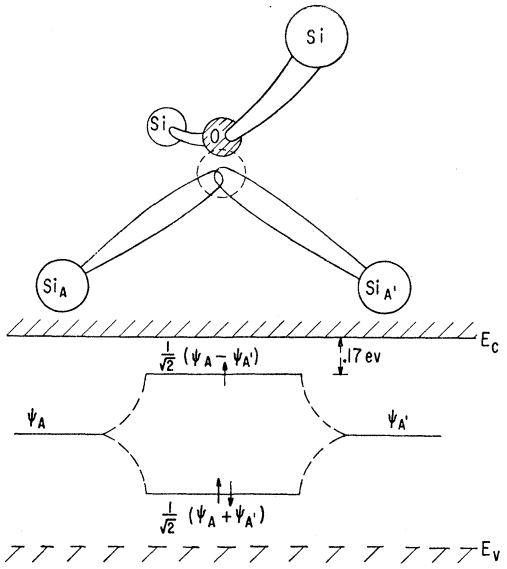


FIG. 6. The Si—Si bond considered as a simple diatomic molecule. In the neutral state, two electrons (one contributed by each atom) are paired off in the bonding orbital. The additional trapped electron goes into the antibonding orbital at ($E_c-0.17$ ev).

We thus conclude that the diatomic Si—Si molecular orbital on the $A$ sites constitutes approximately 70% of the wave function ($\eta_A^2=35\%$ on each of the two $A$ sites). The remainder of the wave function is spread over approximately 12 to 16 neighboring sites. We have not succeeded in identifying to which specific sites in the vicinity of the center these correspond. The fact that the $B$, $C$, and $D$ sets have the same hyperfine axes is quite pertinent. We may conclude from this fact coupled with the number of equivalent $B$ and $C$ sites that the $B$ and $C$ sites must be in the plane of the $Si_A-Si_{A'}$ molecule. It is tempting to argue that they are the next atoms proceeding out from the $A$ sites along the "chain" in the [011] direction for the defect of Fig. 5. This argument, however, cannot be viewed as conclusive.

It might be hoped that a guide to the identity of these sites might come by approximating the nonlocalized part (30%) of the wave function by linear combinations of states from the six ⟨100⟩ valleys of the conduction band in silicon. Such an approach has been highly successful for the shallow impurity donors in silicon.[43] The fact that the $A$ center electron level ($E_c-0.17$ ev) is much deeper than the shallow donors $\sim(E_c-0.05$ ev) makes the approximation poorer in this case. However, one might still hope to obtain some hint as to site identity by such an approach. One can immediately rule out contributions from the valleys along the [100] direction (see Fig. 5) since the corresponding wave functions belong to a symmetry point group that cannot give the required antibonding character. Unfortunately,

[42] L. Pauling, *The Nature of the Chemical Bond* (Cornell University Press, Ithaca, New York, 1948), 2nd ed., Chap. 3.

[43] W. Kohn, in *Solid State Physics*, edited by F. Seitz and D. Turnbull (Academic Press, Inc., New York, 1957), Vol. 5, p. 258.

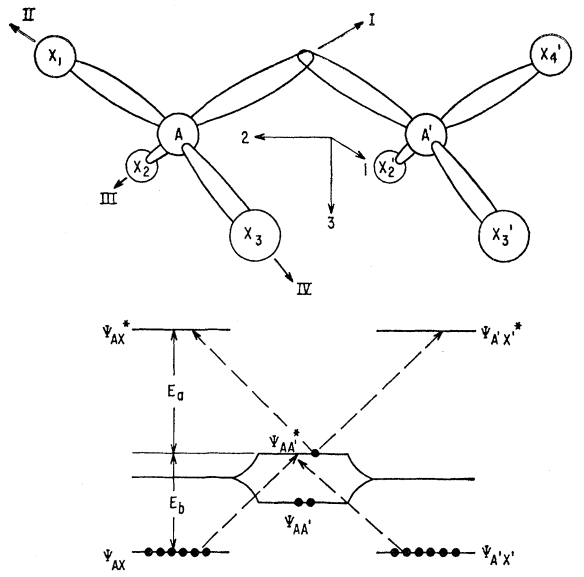


FIG. 7. Localized excited charge transfer states considered in the $g$ shift calculation for the $A$ center.

contributions from the remaining valleys do not appear to single out any particular sites unambiguously to correspond to the $B-E$ sites. They do not even predict the $\langle 111\rangle sp^3$ character clearly indicated in the hyperfine interaction.

We are thus at present of the opinion that the detailed description of the electron wave function will be more readily obtained by using molecular orbital theory throughout, coupled with considerations of the lattice distortions around the defect. We will see in the next section that the lack of more detailed knowledge of the wave function does not represent a significant impasse, since we will satisfactorily account for the observed $g$ tensor by approximating the wave function as completely localized on the $A-A'$ sites.

### 3. $g$ Tensor

To first order in the spin orbit interaction $\lambda\mathbf{L}\cdot\mathbf{S}$, the shift in the $g$ tensor from the free electron value $(g_0)_{ij}=2.0023\delta_{ij}$ is given by[31,44]

$$\Delta g_{ij}=-2\lambda\Lambda_{ij}, \tag{10}$$

where

$$\Lambda_{ij}=\sum_n \frac{\langle 0|L_i|n\rangle\langle n|L_j|0\rangle}{E_n-E_0}. \tag{11}$$

The sum must be taken over all excited states of the defect. It would be a formidable task to try to treat Eq. (11) in detail, including all of the excited states of the solid. However, since the electronic wave function is highly localized, with approximately 70% on the two $Si_A$ sites, a reasonable first approximation would be to consider only localized molecular states.

[44] M. H. L. Pryce, Proc. Phys. Soc. (London) **A63**, 25 (1950).

Let us consider then the eight-silicon molecule shown in Fig. 7. This is made up of the two $A$ atoms plus the six additional atoms bonded to them (three to each). The $A$ atoms make three strong bonds to their nearest neighbor $X$ sites[45] and a weak bond between themselves. In the ground state, there are thus 12 electrons in the filled $\Psi_{AX}$ and $\Psi_{A'X'}$ bonding orbitals, two electrons in the filled $\Psi_{AA'}$ bonding orbital, and the additional spin resonance electron in the $\Psi_{AA'}{}^*$ antibonding orbital as shown in the figure. In this ground state, we have thus made the simplifying assumption that the unpaired electron is localized on the two $Si_A$ sites only.

The excited states of this molecule which give nonvanishing matrix elements of Eq. (11) are of two types. One is formed by an electron transfer from the bonding $\Psi_{AX}$ and $\Psi_{A'X'}$ orbitals to $\Psi_{AA'}{}^*$; the other by an electron transfer from $\Psi_{AA'}{}^*$ to the antibonding $\Psi_{AX}{}^*$ and $\Psi_{A'X'}{}^*$ orbitals as shown in Fig. 7. The first of these represents a "hole" transfer from the $\Psi_{AA'}{}^*$ level (equivalent to a negative $\lambda$) and therefore gives rise to a *positive* $g$ shift. The second represents an electron transfer (positive $\lambda$) and causes a *negative* $g$ shift. The net shift is a result of the difference between these two competing effects.

Consider the four orthogonal orbitals of the $A$ (or $A'$) atom, $\sigma^{\mathrm{I}}$, $\sigma^{\mathrm{II}}$, $\sigma^{\mathrm{III}}$, and $\sigma^{\mathrm{IV}}$, where the superscript represents the orientation of the directed orbital as shown in Fig. 7. (By $\sigma^{-\mathrm{I}}$, we denote an orbit in the opposite direction from the $\sigma^{\mathrm{I}}$ orbit.) We may then construct the one-electron LCAO molecular orbitals as follows:

$$\begin{aligned}
\Psi_{AA'}{}^* &= (2)^{-\frac{1}{2}}[\sigma^{\mathrm{I}}(A)-\sigma^{\mathrm{II}}(A')],\\
\Psi_{AX_1}{}^* &= [2(1-S)]^{-\frac{1}{2}}[\sigma^{\mathrm{II}}(A)-\sigma^{-\mathrm{II}}(X_1)],\\
\Psi_{AX_1} &= [2(1+S)]^{-\frac{1}{2}}[\sigma^{\mathrm{II}}(A)+\sigma^{-\mathrm{II}}(X_1)],
\end{aligned} \tag{12}$$

with similar expressions for the other $\Psi_{AX}$ and $\Psi_{A'X'}$ orbitals. The strong bond $\Psi_{AX}$ orbitals have been normalized to account for overlap with

$$S=\langle\sigma^{\mathrm{II}}(A)|\sigma^{-\mathrm{II}}(X_1)\rangle. \tag{13}$$

The weaker overlap in the $AA'$ bond has not been included. A typical matrix element of Eq. (11) is

$$\begin{aligned}
&\langle\Psi_{AX_1}|L_i|\Psi_{AA'}{}^*\rangle\\
&\quad=\tfrac{1}{2}(1+S)^{-\frac{1}{2}}\langle\sigma^{\mathrm{II}}(A)+\sigma^{-\mathrm{II}}(X_1)|L_i|\sigma^{\mathrm{I}}(A)\rangle.
\end{aligned} \tag{14}$$

If we consider $\sigma^{\mathrm{II}}(A)$ to be the only orbital on atom $A$ with significant overlap with $\sigma^{-\mathrm{II}}(X_1)$, this can be written

$$\begin{aligned}
&\cong\tfrac{1}{2}(1+S)^{-\frac{1}{2}}\langle\sigma^{\mathrm{II}}(A)+\sigma^{-\mathrm{II}}(X_1)|\sigma^{\mathrm{II}}(A)\rangle\\
&\quad\times\langle\sigma^{\mathrm{II}}(A)|L_i|\sigma^{\mathrm{I}}(A)\rangle\\
&\cong\tfrac{1}{2}(1+S)^{+\frac{1}{2}}\langle\sigma^{\mathrm{II}}(A)|L_i|\sigma^{\mathrm{I}}(A)\rangle.
\end{aligned} \tag{15}$$

[45] The distortion caused by the vacancy and the $AA'$ bond will destroy the equivalence of the bond energy in the three different $AX$ orbitals. The in-plane bond (along the II direction in Fig. 7) will probably be stretched the most and, as a result, be weakened. For simplicity, however, we will treat these bonds as equal in strength.

In this way, the matrix elements are reduced to atomic ones. From the symmetry of the center, the principal axes of the molecule are the 1, 2, 3 axes shown in the figure and the $g$ shift along these axes is therefore given by

$$\Delta g_i \equiv \Delta g_{ii} \cong |\lambda| \left\{ \frac{(1+S)}{E_b} - \frac{(1-S)}{E_a} \right\} \times \langle \sigma^{\mathrm{I}}(A) | L_i^2 | \sigma^{\mathrm{I}}(A) \rangle, \quad (16)$$

where $E_a$ is the energy separation between $\Psi_{AA'}{}^*$ and $\Psi_{AX}{}^*$ and $E_b$ that between $\Psi_{AA'}{}^*$ and $\Psi_{AX}$. Here use has been made of the fact that

$$\sum_{m=\mathrm{I}}^{\mathrm{IV}} \langle \sigma^{\mathrm{I}}(A) | L_i | \sigma^m(A) \rangle \langle \sigma^m(A) | L_i | \sigma^{\mathrm{I}}(A) \rangle = \langle \sigma^{\mathrm{I}}(A) | L_i^2 | \sigma^{\mathrm{I}}(A) \rangle. \quad (17)$$

As in Eq. (7), we take a hybrid orbital

$$\sigma^{\mathrm{I}}(A) = \alpha_A (\psi_{3s})_A + \beta_A (\psi_{3p})_A, \quad (18)$$

where the $3p$ orbital is directed along the I axis. The I axis is perpendicular to the 1 axis and makes an angle $\theta = \cos^{-1}(3^{-\frac{1}{2}})$ with respect to the 3 axis (see Fig. 7).

The matrix elements of $L_i^2$ are therefore easily shown to be

$$\begin{aligned} &\langle \sigma^{\mathrm{I}}(A) | L_1^2 | \sigma^{\mathrm{I}}(A) \rangle = \beta_A{}^2, \\ &\langle \sigma^{\mathrm{I}}(A) | L_2^2 | \sigma^{\mathrm{I}}(A) \rangle = \beta_A{}^2 \cos^2\theta = \tfrac{1}{3}\beta_A{}^2, \\ &\langle \sigma^{\mathrm{I}}(A) | L_3^2 | \sigma^{\mathrm{I}}(A) \rangle = \beta_A{}^2 \sin^2\theta = \tfrac{2}{3}\beta_A{}^2. \end{aligned} \quad (19)$$

The observed $\Delta g_1 = +0.0070$. If we use $\beta_A{}^2 = 0.63$ (Table II), $|\lambda| = 0.02$ ev,[46] $S = 0.7$,[47] and assume $E_a \approx E_b$, we may solve Eqs. (16) and (19) for these energies. The result is

$$E_a \approx E_b = 2.6 \text{ ev}. \quad (20)$$

This is a quite reasonable result corresponding to an energy difference between the bonding and antibonding states of approximately 5 ev. The magnitude and sign of the $g$ shift is thus satisfactorily accounted for by the model. (The positive $g$ shift arises primarily as a result of the overlap integral $S$ in Eq. (16) which expresses the fact that the unpaired electron interacts more strongly with the bonding $AX$ orbitals than the antibonding ones.[48]) Equation (19) predicts $\Delta g_1 : \Delta g_3 : \Delta g_2 = 3:2:1$. The observed values are $\Delta g_1 = +0.0070$, $\Delta g_3 = +0.0008$, $\Delta g_2 = +0.0002$. These depart significantly from the predicted ratios but at least are in order $\Delta g_1 > \Delta g_3 > \Delta g_2$ as predicted.

This simple localized molecular model is thus capable of explaining the magnitude and signs of the $g$ shift in a reasonably satisfactory way. We do not expect detailed agreement because only approximately 70% of the wave function is involved in the diatomic $\mathrm{Si}_A - \mathrm{Si}_{A'}$ molecule we have treated. The contribution of the remaining 30% has not been treated. [Even within the framework of the localized molecular states considered here, a more detailed treatment could alter the relative values of $\Delta g_i$ to some extent. Such a treatment could include the effect of overlap between the $A$ and $A'$ orbitals and between $\sigma^{-\mathrm{II}}(X_1)$ and orbitals other than $\sigma^{\mathrm{II}}(A)$ which were ignored in Eq. (15). Also, allowance could be made for values of $E_b$ and $E_a$ for the $AX_1$ orbital different from those for the $AX_2$ and $AX_3$ orbitals.] Indeed, the agreement is rather remarkable when one considers that even though this electron state is only 0.17 ev from the conduction band, it can be treated with considerable success, completely ignoring the fact that it is in a semiconductor at all.

## IV. EFFECTS OF AXIAL STRESS

### A. General

There are six possible orientations of the $A$ center in the cubic silicon lattice corresponding to the 3! different

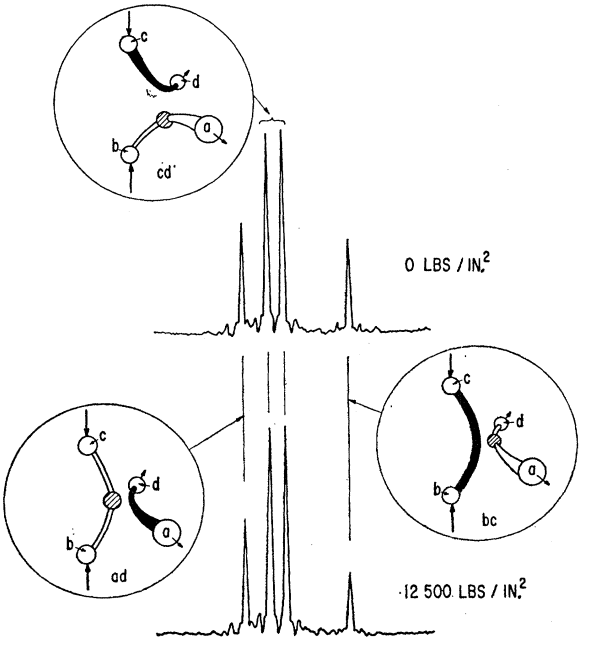


FIG. 8. Change in the spectrum resulting from electronic redistribution under ⟨110⟩ stress at 77°K. The insets show the defect orientation corresponding to each multiplet. The decrease of the *bc* multiplet under stress confirms that the electron is in an antibonding orbital.

[46] As in the $|\psi_{3s}(0)|^2$ estimate for the hyperfine interaction, we estimate that $|\lambda|$ is the value appropriate to $\mathrm{Si}^0$. From *Atomic Energy Levels*, edited by C. E. Moore, National Bureau of Standards Circular No. 467, (U. S. Government Printing Office, Washington, D. C., 1949), this is two-thirds the energy difference between the $P_{\frac{3}{2}}$ and $P_{\frac{1}{2}}$ level giving $|\lambda|$ as ~0.02 ev.

[47] Estimated assuming tetrahedral hybrid orbitals ($sp^3$) and the normal lattice Si−Si bond distance (2.35 A) from the tables given by R. S. Mulliken, C. A. Rieke, D. Orloff, and H. Orloff, J. Chem. Phys. **17**, 1248 (1949).

[48] The $g$ shifts in organic free radicals are also positive. The situation there is completely analogous to the one here, the $g$ shift arising from matrix elements of $L_i$ between the unpaired $\pi$ electron and the bonding $\sigma$ states of the same atom. H. M. McConnell and R. E. Robertson, [J. Phys. Chem. **61**, 1018 (1957)] have suggested that this reflects the fact that $E_a > E_b$, i.e., that the antibonding state is more antibonding than the bonding state is bonding. This is true, but the effect of overlap, which they did not consider, is probably more important.

ways the oxygen atom can be placed between two of the four silicon atoms surrounding a vacancy (see Fig. 5). Because of the anisotropy in $g$, for an arbitrary orientation of the crystal in the magnetic field, these six differently oriented defects will give rise to six separate resonance lines, each being identified with a particular defect orientation. These lines will be equally intense because each orientation is entirely equivalent to the others.

However, if a uniaxial stress is applied to the crystal, the crystal is distorted from its normal cubic symmetry and the six differently oriented defects are no longer equivalent. Correspondingly, we find that the relative intensities of the lines change under the applied stress. Two mechanisms are found for this change. First, the energy of the electron trapped at the $A$ center is raised or lowered depending upon the orientation of the defect with respect to the stress. The intensities therefore can change as a result of electronic redistribution between the defects. Second, at a sufficiently elevated temperature, the defects themselves can reorient thermally and will seek a preferential orientation with respect to the applied stress.[49] These two effects occur in different temperature regions and are therefore readily separable. In the following sections, we will consider first the electronic redistribution and then the defect reorientation in detail.

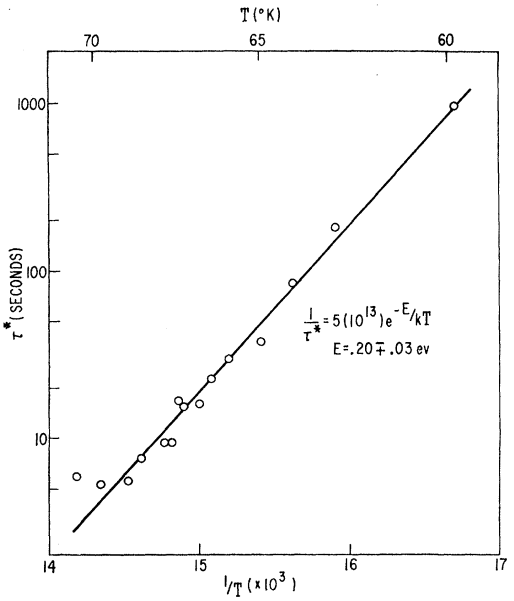


FIG. 9. The rate of electronic redistribution between $A$ centers vs temperature. The characteristic relaxation time $\tau^*$ is measured by observing the recovery of the spectrum after the stress is removed.

[49] The observation by spin resonance of the reorientation of defects under uniaxial stress was first made by G. W. Ludwig and H. H. Woodbury for $Ni^-$ in germanium (unpublished).

## B. Experimental Results and Discussion

### 1. *Electronic Redistribution*

Figure 8 shows the change in the spectrum resulting from an applied stress along a ⟨110⟩ direction at 77°K. That this results from electronic redistribution between the differently oriented defects is demonstrated by the fact that no change is observed when the number of centers are less than or equal to the original number of phosphorus donors. In this case, each $A$ center traps an electron and is thus observed in the resonance, pressure on or off. The failure to observe amplitude changes in this case proves that the defect itself is not reorienting. The amplitude changes shown in Fig. 8 result only when the sample is irradiated sufficiently so that the $A$ centers exceed the number of original donors. In this case, the electrons can redistribute between the traps (by thermal ionization) and seek out the lower energy ones. In the samples used for this study, the $A$ center concentration was approximately 10 times the phosphorus concentration.

The rate at which this redistribution occurs was studied in the temperature region 60° to 70°K by monitoring the recovery after the pressure was removed. A simple exponential recovery was observed with the characteristic relaxation time varying with temperature as shown in Fig. 9. This relaxation time is equal to the average time an electron spends trapped at a defect between ionization events and is given by

$$(\tau^*)^{-1}=5(10^{13})\exp(-E/kT)\ \text{sec}^{-1},$$

with

$$E=0.20\pm0.03\ \text{ev}.$$

The frequency factor is a characteristic lattice vibration frequency and the activation energy is close to the trap level position at 0.17 ev. (The slightly higher value for the activation energy, though not outside experimental error, could represent a real difference. The level position at 0.17 ev is measured from steady state conductivity and Hall measurements vs temperature and measures the position of the level below the conduction band. The transient rate of recovery measures the height of the barrier for the electron to get out. Since the defect is negatively charged when an electron is trapped, a slight excess barrier may exist resulting from the Coulomb energy associated with the concentration of charge.)

Because the $A$ center concentration greatly exceeds the electron donor concentration (10×), the relative electron population for the differently oriented defects is given closely by a Boltzmann distribution between them. This is illustrated in Figs. 10(a)–(c) for samples stressed along the three principal crystal axes: ⟨110⟩, ⟨100⟩, and ⟨111⟩, respectively. (In the figures, the four silicon atoms surrounding the vacancy are labeled $a$ through $d$. By the subscript $ad$ we denote the defect for which the electron trap is shared between the $a$ and $d$

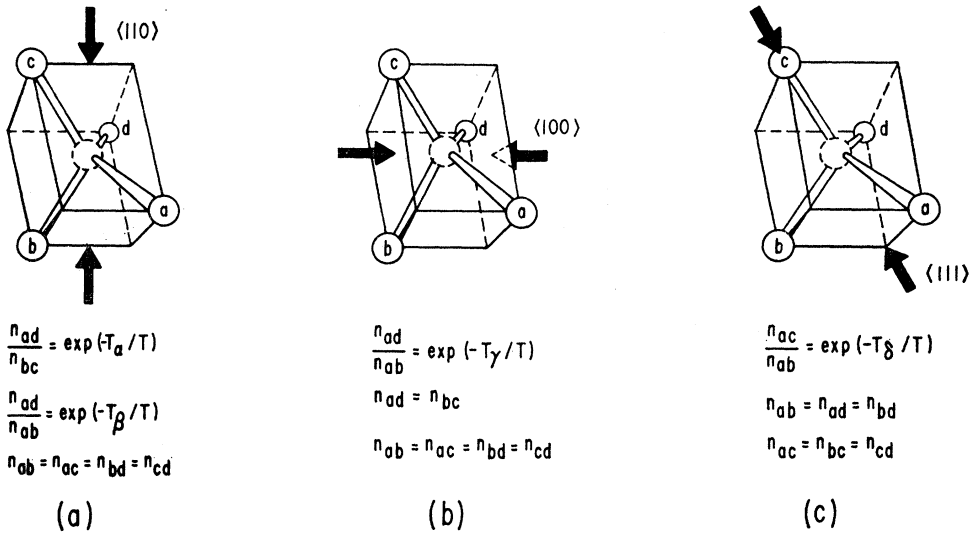


FIG. 10. Boltzmann factors governing the populations of the different defect orientations for the separate (a) ⟨110⟩, (b) ⟨100⟩, and (c) ⟨111⟩ stress experiments. The subscript $ij$ refers to the defect for which the electron trap is shared between the $i$ and $j$ silicon atoms.

silicon atoms.) For a ⟨110⟩ stressed crystal, there are three nonequivalent orientations for the defect. Two energy differences are therefore required to describe the Boltzmann distribution between them and they are taken as $kT_\alpha^*$ and $kT_\beta^*$, as described in Fig. 10(a). (The asterisk will be used for the electron trap energy differences determined in this section.) For the ⟨100⟩ and ⟨111⟩ stressed samples, only two nonequivalent orientations result and a single energy for each, $kT_\gamma^*$ and $kT_\delta^*$, respectively, is required. The relative amplitudes at 77°K under a stress of 12 500 psi in crystals stressed in each of these three directions were studied; the values of $T_\alpha^*$, $T_\beta^*$, $T_\gamma^*$, and $T_\delta^*$ determined for this applied pressure are given in Table IV.

A detailed consideration of these energy differences will be described in Sec. IV(C). However, at this point, an important observation can be made. From the signs of the observed energy differences we conclude that the trap energy is raised when the two silicon atoms of the Si—Si diatomic molecule are pushed together. This is seen easily in Fig. 8, where the resonance intensity is observed to decrease for the defect in which the two trapping silicon atoms are pushed together. This confirms that the electron trap is an antibonding orbital between these two silicon atoms. (In Fig. 6, it is seen that pushing the two silicon atoms together lowers the energy of the bonding orbitals; raises that of the antibonding ones.)

### 2. *Defect Orientation*

At higher temperatures, the defects themselves can reorient thermally and seek a preferred orientation in the strained crystal. This causes an additional change in the amplitudes of the lines in the spectrum which is easily separated from that resulting from the faster electronic redistribution.

In order to study this effect quantitatively we must first recognize the fact that the $A$ center is a different defect depending upon whether it has trapped an electron (charged) or not (neutral). The rate at which the defect reorients, as well as the degree of preferential alignment, will be different for the two charge states. As a result we have chosen to study the properties of the neutral state. In order to do this, the experiments were again performed on samples in which the $A$ center concentration was approximately 10 times that of the phosphorus. In this way, approximately 90% of the time an individual defect does not have a trapped electron and its average[50] properties thus reflect closely

TABLE IV. Comparison of the observed and calculated energy differences (in °K) for the differently oriented defects under stress (see Fig. 10). The $T_j$ refer to the relative stability of the different defect orientations and the $T_j^*$ refer to the differences in energy of the electron trap associated with each defect orientation. The applied stress is 12 500 psi.

| Stress | $T_j$ | Observed (°K) | Calculated (°K) |
|---|---|---|---|
| ⟨110⟩ | $T_\alpha$ | −8 | −7 |
| | $T_\alpha^*$ | −47 | −51 |
| | $T_\beta$ | −84 | −87 |
| | $T_\beta^*$ | −3 | −5 |
| ⟨100⟩ | $T_\gamma$ | +164 | +164 |
| | $T_\gamma^*$ | −42 | −40 |
| ⟨111⟩ | $T_\delta$ | +4 | +4 |
| | $T_\delta^*$ | +33 | +35 |

[50] Because the reorientation rate of the defect is many orders of magnitude slower than the electronic redistribution rate, a single defect has trapped and thermally released an electron many times over the characteristic time of reorientation. We are thus concerned with average properties, i.e., 90% neutral, 10% charged.

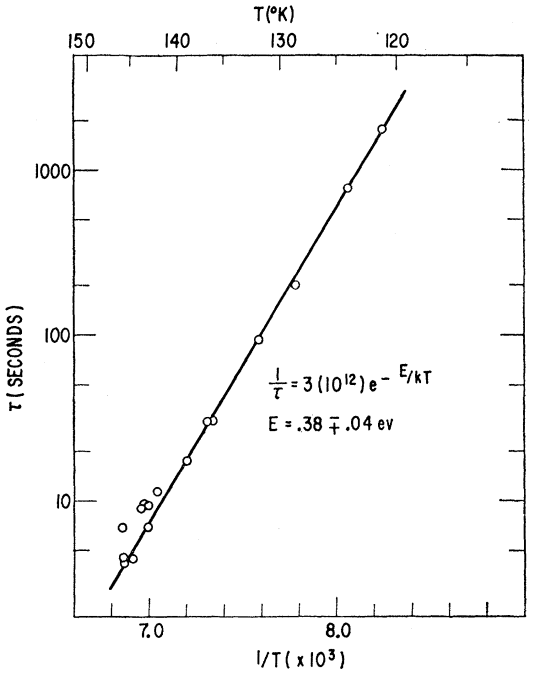


FIG. 11. The rate of $A$ center reorientation vs temperature. The characteristic relaxation time $\tau$ is measured by observing the recovery of the spectrum after the stress is removed.

those of the neutral state. The electrons are used then only as a means of sampling the defects without significantly altering their properties.

The rate at which the neutral defect reorients was studied by measuring the recovery after pressure was removed in the temperature region 120°–145°K. The crystal was originally stressed in the ⟨110⟩ direction and the recovery of the $ab+ac+bd+cd$ defects (see Fig. 10) was observed. After an initial "instantaneous" electronic recovery, the slower reorientation followed a simple exponential recovery. The results are given in Fig. 11. The characteristic relaxation time $\tau$ was determined to be

$$\tau^{-1}=3(10^{12})\exp(-E/kT)\ \text{sec}^{-1},$$

with

$$E=0.38\mp0.04\ \text{ev}.$$

For the model of Fig. 5, this activation energy is the barrier the oxygen atom must overcome to switch to another pair of silicon atoms surrounding the vacancy. A value of approximately 0.4 ev does not appear unreasonable, the probable motion being to break one Si—O bond while pivoting around the other.[51]

The magnitude of the effect is shown in Fig. 12. The sample studied in this figure has been quenched from 125° to 77°K with the pressure on and then observed with the pressure removed. When the pressure is removed, the polarization associated with the electronic redistribution disappears, leaving only that resulting from the defect reorientation frozen in. The relative amplitudes of the lines reflect the relative number of correspondingly oriented defects at the temperature of quench (125°K). These in turn are given by a Boltzmann distribution between the various orientations at this temperature. Using this quench technique, and a stress of 12 500 psi, the results for $T_\alpha$, $T_\beta$, $T_\gamma$, and $T_\delta$ of Fig. 10 were determined and are as given in Table IV.

These results will be analyzed in detail in the next section but again a few qualitative observations can be made. From the model (Fig. 5) we expect the orientation preference to be determined primarily by the Si—O—Si molecular bond and the corresponding Si—Si molecular bond across the vacancy from it. Each is a stretched bond[52] and therefore lowers its energy by aligning its bond axis along the direction in which the crystal is compressed.

This is clearly indicated in Fig. 12. The $ad$ orientation is enhanced because the Si—O—Si bond is aligned along the direction of squeeze. The $bc$ orientation is also enhanced because it presents the Si—Si bond axis along the direction of squeeze. They are enhanced at the expense of the other orientations because the other orientations have little resolved strain along these two molecular axes. Similarly, the near zero value of $T_\delta$ results from the fact that the two bonds are competing directly [see Fig. 10(c)] for this ⟨111⟩ squeeze. The large value of $T_\gamma$ for the ⟨100⟩ squeeze, on the other hand, results from the fact that the two bonds are both stretched for one of the two nonequivalent defect orientations, and compressed for the other, their effects adding.

### C. Analysis of the Data

Let us assume the following:

(a) The change in energy of the electron trap is determined primarily by the change in the $Si_A-Si_{A'}$ distance in the strained lattice. We define the change in this energy per unit strain along this direction as

$$M^*=[(dE/d\epsilon)^*]_{\text{Si-Si}}. \tag{21}$$

(b) The relative stability of the different defect orientations is determined by the competition between the Si—O—Si and $Si_A-Si_{A'}$ molecular bonds to align along the compressed direction. Further, the change in energy of each bond is primarily determined by the component of strain along the bond axis. We thus define

[51] The exact relation between the observed relaxation time $\tau$ and the time characteristic of the microscopic jump process depends in detail upon the jumps involved. If the dominant jump involved is this pivoting process, the lifetime between jumps can be shown to be $(3/2)\tau$ for the particular ⟨110⟩ stress recovery experiment performed here.

[52] The Si—O distance for an oxygen atom placed at the center of the vacancy is 40% greater than the Si—O distance in a free molecule. Similarly, the Si—Si bond is between normal next-nearest neighbors and therefore gains energy by bringing the silicon atoms closer together. Since these two axes are at right angles we expect the relative stability of each orientation to be the result of the competition between these two bonding halves to align along the compressed direction.

two additional parameters

$$M=(dE/d\epsilon)_{\text{Si-Si}}, \tag{22}$$

$$N=(dE/d\epsilon)_{\text{Si-O-Si}}. \tag{23}$$

With these assumptions, we may calculate the various $T$ and $T^*$ of Table IV as follows:

### 1. ⟨100⟩ Stress

Under stress, the electron trap on the $ij$ silicon atoms (see Fig. 10) is changed in energy by the amount $M^*\epsilon_{ij}$, where $\epsilon_{ij}$ is the fractional strain along the line joining the $i$ and $j$ silicon atoms. The resulting energy difference between the trap energies of the $ad$ orbital and the $ab$ orbital (by definition, $kT_\delta^*$) is given therefore by

$$kT_\delta^*=(\epsilon_{ad}-\epsilon_{ab})M^*. \tag{24a}$$

Both $M$ and $N$ contribute in determining $T_\delta$. The $ad$ defect (electron trap between the $a$ and $d$ silicon atoms) is changed in energy by $M\epsilon_{ad}$ contributed from the Si—Si bond and $N\epsilon_{bc}=N\epsilon_{ad}$ from the Si—O—Si bond. The energy of the $ab$ defect is similarly changed by $\epsilon_{ab}(M+N)$, giving

$$kT_\delta=(\epsilon_{ad}-\epsilon_{ab})(M+N). \tag{24b}$$

The fractional strains $\epsilon_{ab}$ and $\epsilon_{ad}$ can be computed in terms of the elastic moduli ($s_{11},s_{12},s_{44}$) and applied pressure $P$ by conventional means[53] and are given by

$$\epsilon_{ad}=\epsilon_{bc}=-s_{12}P, \tag{25a}$$

$$\epsilon_{ab}=\epsilon_{ac}=\epsilon_{bd}=\epsilon_{cd}=-\tfrac{1}{2}(s_{11}+s_{12})P. \tag{25b}$$

### 2. ⟨110⟩ Stress

A similar calculation gives

$$kT_\alpha^*=(\epsilon_{ad}-\epsilon_{bc})M^*, \tag{26a}$$

$$kT_\beta^*=(\epsilon_{ad}-\epsilon_{ab})M^*, \tag{26b}$$

$$kT_\alpha=(\epsilon_{ad}-\epsilon_{bc})(M-N), \tag{26c}$$

$$kT_\beta=(\epsilon_{ad}-\epsilon_{ab})M+(\epsilon_{bc}-\epsilon_{ab})N, \tag{26d}$$

with

$$\epsilon_{ad}=-\tfrac{1}{4}P(2s_{11}+2s_{12}-s_{44}), \tag{27a}$$

$$\epsilon_{bc}=-\tfrac{1}{4}P(2s_{11}+2s_{12}+s_{44}), \tag{27b}$$

$$\epsilon_{ab}=\epsilon_{ac}=\epsilon_{bd}=\epsilon_{cd}=-\tfrac{1}{4}P(s_{11}+3s_{12}). \tag{27c}$$

### 3. ⟨111⟩ Stress

Similarly,

$$kT_\delta=(\epsilon_{ac}-\epsilon_{ab})(M-N), \tag{28a}$$

$$kT_\delta^*=(\epsilon_{ac}-\epsilon_{ab})M^*, \tag{28b}$$

with

$$\epsilon_{ac}=\epsilon_{bc}=\epsilon_{cd}=-\tfrac{1}{6}P(2s_{11}+4s_{12}+s_{44}), \tag{29a}$$

$$\epsilon_{ab}=\epsilon_{ad}=\epsilon_{bd}=-\tfrac{1}{6}P(2s_{11}+4s_{12}-s_{44}). \tag{29b}$$

[53] W. Voigt, *Lehrbuch der Kristallphysik* (B. G. Teubner, Leipzig, Germany, 1928), p. 589 ff.

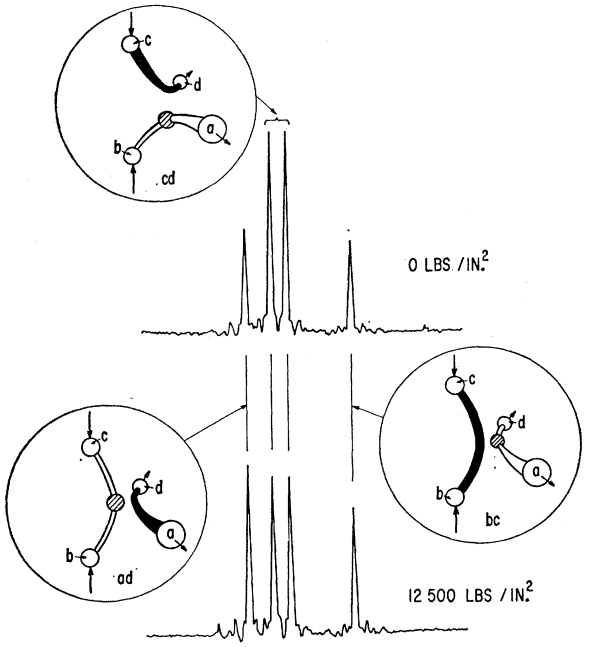


FIG. 12. Change in the spectrum resulting from $A$ center reorientation under ⟨110⟩ stress. (The stress was applied at 125°K and the resulting alignment was frozen in by quenching to 77°K where the spectra were taken). The insets show the defect orientation corresponding to each multiplet.

With $s_{11}=7.68\times10^{-13}$, $s_{12}=-2.14\times10^{-13}$, and $s_{44}=12.56\times10^{-13}$ cm²/dyne,[54] selection of $M^*$, $M$, and $N$ for the best fit of Eqs. 24–29 with the data of Table IV gives:

$$M=[(dE/d\epsilon)]_{\text{Si-Si}}=+16.0 \text{ ev/unit strain},$$

$$N=[(dE/d\epsilon)]_{\text{Si-O-Si}}=+17.2 \text{ ev/unit strain}, \tag{30}$$

$$M^*=[(dE/d\epsilon)^*]_{\text{Si-Si}}=-8.0 \text{ ev/unit strain}.$$

The values computed with these constants are given in Table IV.

The magnitudes of $M$, $M^*$, and $N$ appear reasonable, being of the same order of magnitude as deformation potentials in silicon.[55] In addition, the fact that $M^*=-\frac{1}{2}M$ is an important confirming feature of the model: $M^*$ is the change in energy per unit strain for a single electron in an antibonding $Si_A-Si_{A'}$ orbital. It should therefore be of the opposite sign and approximately half the value of $M$, which is that for two electrons in the bonding orbitals.

Considering this additional relation behind $M$ and $M^*$, it has thus been possible to predict in sign and magnitude all eight observed energy differences in Table IV with only two parameters: $M$ and $N$, both of reasonable magnitude. This must be considered strong confirmation of the model.

[54] H. B. Huntington, in *Solid State Physics*, edited by F. Seitz and D. Turnbull (Academic Press, Inc., New York, 1958), Vol. 7, p. 274.

[55] C. Herring and E. Vogt., Phys. Rev. **101**, 944 (1956).

## V. SUMMARY

The spin resonance studies outlined in this paper substantiate many of the features of the model of the $A$ center as a substitutional oxygen atom. The $A$ center is presumably formed when a mobile lattice vacancy (produced by the irradiation) is trapped by an interstitial oxygen atom impurity. The detailed model deduced from these studies is one in which the oxygen atom bonds to two of its four nearest silicon neighbors, with the remaining two silicon neighbor atoms pulling together to form a covalent bond. An additional electron can be trapped in an antibonding orbital of this Si—Si molecule at ($E_c-0.17$ ev) and it is this additional electron that is observed in the spin resonance. The primary confirming features in the spin resonance are summarized as follows:

1. Analysis of the resolved hyperfine interactions with $Si^{29}$ nuclei indicates that approximately 70% of the wave function of the trapped electron is localized on two silicon atoms. The magnitude and symmetry of the hyperfine interactions on these sites is in good agreement with that predicted for the two bonding silicon atoms adjacent to the vacancy in the model. (The remaining 30% of the wave function is spread over approximately 12 to 16 neighboring sites.)

2. The magnitude and symmetry of the $g$ tensor has been satisfactorily accounted for in terms of the model.

3. Studies of electronic redistributions between the $A$ centers under uniaxial stress confirms that the electron is in an antibonding orbital. The rate of redistribution vs temperature has also been studied, giving an activation energy close to the level position at ($E_c-0.17$ ev).

4. The thermally activated switching of the oxygen atom from one pair of silicon atoms to another in the vacancy has been observed indirectly by observing the preferential alignment of the defects resulting from uniaxial stress. The activation energy for this motion is $0.38\mp0.04$ ev for the neutral charge state of the defect.

5. It is possible to account quantitatively for the observed defect alignment as well as the magnitude of the preferred electronic redistribution by a simple analysis of how the defect distorts under stress. This analysis involves resolving the applied strain along the two orthogonal bonding axes (Si—Si and Si—O—Si) and, using a single experimentally determined value for the change in energy of each bond in terms of the strain along its axis, calculating the resulting stability of each orientation. The magnitude of these constants is reasonable, being of the order of observed deformation potentials.

The oxygen atom has not been observed directly in the resonance studies. Its presence is only inferred. In the following paper,[12] an infrared absorption band at 12 $\mu$ will be identified as arising from the vibration of this oxygen atom. By studying the effect of stress on the absorption band and by comparison with the stress experiments described in this paper, it will be possible to prove conclusively the existence of the oxygen atom and also confirm the detailed model as to how the oxygen is incorporated in the defect.

## VI. ACKNOWLEDGMENTS

The authors are indebted to Dr. R. O. Carlson for supplying most of the silicon samples used in this study. Mr. W. Colliton materially assisted in all phases of the measurements. Helpful conversations with Dr. G. W. Ludwig concerning the stress experiments and Dr. B. Segall concerning the nature of the band structure in silicon are also gratefully acknowledged.